ISSN: 2643-6876

Current Trends in Civil & Structural Engineering

DOI: 10.33552/CTCSE.2025.12.000776

Iris Publishers

Review Article

Experiments and Numerical Analysis of Crane Toppling Using Ultra-Small Model

Shouji Toma[1]* and Wai Fah Chen[2]

[1]Emeritus Professor, Hokkai Gakuen University, Japan, Taiki Consultant, Inc., Sapporo Office, Japan

[2]Emeritus Professor., University of Hawaii, USA

***Corresponding author:** Shouji Toma, Emeritus Professor, Hokkai Gakuen University, Japan

Received Date: November 17, 2025

Published Date: December 05, 2025

Abstract

Recent studies have suggested that toppling accidents involving cranes and pile drivers are influenced not only by overturning moment but also by structural instability. To investigate this phenomenon, theoretical analyses have been conducted using a simplified structural model composed of a rigid bar and a rotational spring system. Extensive numerical simulations were performed by varying the initial inclination angle and boom length under different supporting ground stiffness conditions, thereby examining the contribution of structural instability to toppling behavior. In this study, the analytical findings derived from these simplified models are experimentally validated through toppling tests using an ultra-small-scale crane model. Although the use of a miniature model limits experimental precision, it provides a practical advantage by enabling a wide range of test conditions to be evaluated with ease. The experimental results confirm the validity of the previously proposed analytical approach that considers both structural instability and overturning moment in defining the toppling condition. Furthermore, the findings contribute to a clearer understanding of the underlying mechanisms governing crane toppling.

Keywords: Crane toppling; pile driver toppling; structural instability of heavy machinery; toppling mechanism; initial inclination angle; crane stability; toppling experiment

Introduction

A significant number of toppling accidents in various structures are thought to involve structural instability. Examples include bridge girder drops caused by jack overturning [1,2], as well as heavy machinery toppling accidents involving cranes and pile drivers [3]. These incidents suggest that not only overturning moments but also structural instability play a role, motivating theoretical studies based on structural stability theory [4,5]. In these studies, in addition to conventional static analyses, the influence of dynamic inertial forces in facilitating toppling has also been highlighted [6,7]. Recent research has examined crane operational parameters, such as working height and radius, and evaluated toppling safety criteria under these conditions, considering factors such as suspended loads and supporting ground stiffness [8]. Numerical analyses incorporating structural instability have further explored the relationships among load magnitude, load height, ground stiffness, and toppling conditions [9]. The present study aims to

experimentally validate the toppling conditions obtained from these numerical analyses. To achieve this, various experiments were conducted using an ultra-small-scale crane model. This paper first presents an overview of the experimental setup, including the miniature model used, followed by an analysis and discussion of the toppling test results from multiple perspectives. The study provides empirical data on toppling behavior and clarifies the role of structural instability in crane and pile driver toppling accidents, thereby contributing to future accident prevention measures.

Toppling Experiment Overview

Ultra-Small-Scale Experimental Model

The ultra-small-scale crane model used in the experiments is shown in Figure 1, with its specifications summarized in Table 1. The commercially available miniature model is based on a large-scale building demolition machine originally designed for structures approximately 65 m in height (equivalent to 21 stories). With a scale ratio of 1:228, the model has a boom length of approximately 30 cm, a total mass of 65.5 g, and a crawler center-to-center distance of 3.3 cm. Due to its extremely small size, accuracy compared to full-scale behavior and reproducibility on soft ground may be poor. Nevertheless, the simplicity and compactness of the model allow for experiments under a variety of conditions, facilitating the evaluation of the effects of changes in experimental parameters. Figure 1 also indicates the locations of the suspended loads and the corresponding basic toppling test cases. For reference, the structural appearance of the machine's lower section as seen from the front is shown in Photograph 2 in Appendix. Although the original machine was a building demolition machine and thus has a slightly different boom tip configuration compared to conventional cranes, the fundamental structural characteristics are preserved. Therefore, the influence of this difference on the primary objective of understanding toppling behavior is expected to be minimal. Additionally, as shown in Figure 1, the experimental model features a non-telescoping boom, so the weight of the crane itself remains constant and does not vary with the position of the suspended load.

Table 1: Ultra-Small Model.

Model Name	Tomica 130 made by Tomy Co. Ltd. (Original: KOBELCO SK3500D Bld. Dem. SK3500D)
Scale	1/228
Boom Length	abt. 30cm
Mass	65.5g
Crawler Spacing	3.3cm

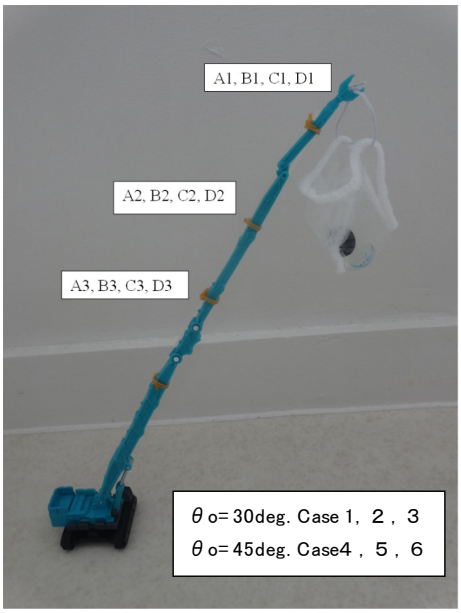

Figure 1: Ultra-Small Model and Loading Positions.

Types of Supporting Foundations and Load Application

Four types of supporting foundations were used to support the crane model, as summarized in Table 2. These were selected in order of hardness:

a. on laptop computer – very stiff

b. on urethane mattress – moderately stiff

c. on towel (folded four times) – slightly soft

d. on cushion – soft

Table 2: Basic Toppling Experiment Conditions.

Experiment Conditions		Toppling Experiments		Numerical Cal.
Foundation	θo	30deg.	45deg.	30deg.
A. Hard	on PC	A1, A2, A3	A4, A5, A6	A1', A2', A3'
B. Slightly Hard	on Mattress	B1, B2, B3	B4, B5, B6	B1', B2', B3'
C. Soft	on Tawel	C1, C2, C3	C4, C5, C6	C1', C2', C3'
D. Very Soft	on Cusshon	D1, D2, D3	D4, D5, D6	D1', D2', D3'

Photographs of the actual supporting foundations are provided in Appendix. For the C. on towel configuration, the towel rests on a hard computer desk, which likely influenced the experimental results. For the D. on cushion, the deformation changes over time due to surface fabric tension and internal air compression. Consequently, load history affects the C. on towel and D. on cushion conditions, resulting in reduced reproducibility. Nevertheless, the experiments are considered sufficiently reliable and provide valuable data on toppling behavior that would be difficult to obtain in full-scale testing. Loads were applied by suspending very lightweight bags from the boom, as shown in Figure 1. Three types of weights were used: glass beads (≒1.5 g), plastic Othello pieces (≒1.2 g), and aluminum 1-yen coins (≒1 g). Suspended loads were applied at three positions along the boom: 1 upper, 2 middle, and 3 lower, as illustrated in Figures 1 and 3. For all tests, the boom rotation angle was fixed at 90° (horizontal direction) to simplify analysis.

Measurement Instruments and Methods

Mass measurements were conducted using a kitchen scale (ELECOM, maximum capacity 2 kg, minimum display 0.1 g) as shown in Figure 2. For cases in which the smallest weight (1-yen coin, 1 g) caused toppling, the pre- and post-toppling conditions were used to estimate the critical load with 0.1 g resolution. Boom height and working radius were measured using a tape measure; digital measurements were not performed. In the basic overturning tests, the initial boom inclination angle was set using a protractor (Photograph 4 in Appendix), and the working radius was calculated from the measured load height. Due to the extremely small scale of the model and the use of analog measurement methods, the absolute precision of the experiments is limited. However, the primary objective of this study—to analyze crane overturning behavior from multiple perspectives using a simple experimental setup—has been largely achieved.

Figure 2: Mass Scale and Weights.

Types of Toppling Experiments

A total of five experimental categories were conducted using the ultra-small-scale crane model, each designed to address specific research objectives.

Basic Toppling Experiments

The first set of experiments, referred to as the basic toppling experiments, examined the influence of supporting foundation, initial boom inclination angle, boom length, working radius, and other parameters on the critical overturning load (toppling load). Four types of supporting foundations, arranged in order of increasing compliance, were used: A. on laptop computer, B. on urethane mattress, C. on towel, and D. on cushion. The initial boom inclination angles were set at [1] θ_0 = 30° and [2] θ_0 = 45° with respect to the vertical axis. Suspended loads were applied at three positions along the boom, as shown in Figure 1 and Figure 3: the uppermost point (load point 1), intermediate point (load point 2), and lowest point (load point 3). Table 2 summarizes the conditions for the basic toppling experiments, and photographs in Appendix illustrate each experimental configuration. The results of the basic overturning experiments provided the basis for four additional experimental categories, each designed to analyze specific aspects of crane toppling behavior, as explained in the following.

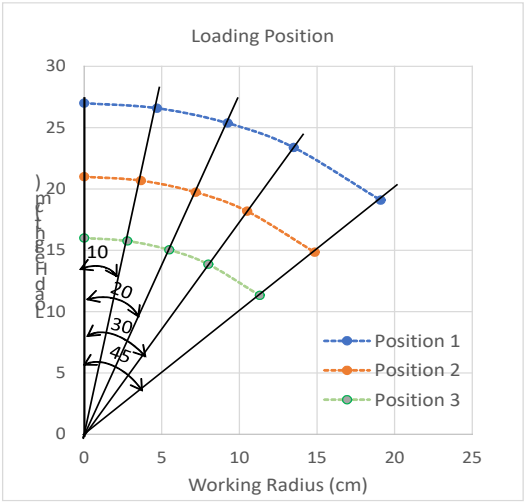

Figure 3: Load Height and Working Radius.

Experiment for Influence of Initial Boom Inclination Angle

The second experimental category investigated the effect of initial boom inclination angle θ_0 on the critical load and other overturning characteristics. These tests were conducted on the C. on towel supporting foundation, with θ_0 varied across five values: 0°, 10°, 20°, 30°, and 45°. In addition to the 30° and 45° cases tested in the basic experiments, supplemental tests were conducted for 0°, 10°, and 20° to enable a comprehensive comparison across all five inclination angles.

Rotational Spring Stiffness Investigation (Fixed Working Radius)

The third experiment measured displacements under a fixed working radius on the C. on towel foundation while varying the initial boom inclination angle for a given load. From these measurements, the rotational spring stiffness of the foundation was estimated and compared, as the stiffness should theoretically be the same for identical supporting conditions. The calculated stiffness values were then used to generate load–displacement angle curves, allowing validation of the experimental methodology. It should be noted that this experiment does not involve toppling; rather, it focuses on the estimation of rotational spring stiffness.

Experiment for Influence of Supporting Foundation (θ_0 = 10°)

The fourth experimental category examined the influence of supporting foundation stiffness at a relatively small initial boom inclination angle (θ_0 = 10°), where structural instability effects are more pronounced. Supporting foundations were varied across four types: computer desk, four-layer towel, six-layer towel, and ten-layer towel. For each foundation type, suspended loads were applied at the three load points (1, 2, and 3), resulting in different working radii due to the constant inclination angle. The objective was to evaluate how foundation compliance affects toppling behavior under small initial tilt conditions.

Structural Instability Influence (Equilibrium-Transition Toppling)

The fifth experimental category focused on toppling behavior influenced by structural instability, specifically equilibrium-transition-type toppling. Experiments were conducted on a

very stiff supporting foundation (wooden board) representing the overturning-moment-dominated case and on a very soft foundation (futon) representing the equilibrium-transition case. The suspended load was applied at the uppermost point (load point 1), where structural instability effects are most pronounced. The working radius was set to a = 8 cm with an initial boom inclination angle of θ_0 = 15.7° for both cases. The magnitude and height of the load at overturning were measured, enabling a direct comparison between overturning-moment-dominated and structural-instability-dominated behaviors. The following sections present and discuss the results of each experimental category.

Results and Discussion of Basic Toppling Experiments

Analysis of Overturning Stability

The results of the basic toppling experiments summarized in Table 2 are presented by supporting foundation type in Tables 3-1 through 3-4: A. on laptop computer, B. on urethane mattress, C. on towel, and D. on cushion. In these tables, the upper-left (shaded blue) values correspond to measured data, while the remaining entries are calculated values derived from a combination of measured data, initial settings (e.g., initial inclination angle), and structural parameters of the model. In each table, the experimental columns [1] (initial inclination angle θ_{01} = 30°) and [2] (θ_{02} = 45°) correspond to the toppling experiment results. The columns on the right, [1′] (toppling) and [1″] (non-toppling), show numerical values calculated from simulations based on these experimental results. The following discussion focuses first on the experimental results in columns [1] and [2].

The first four rows of Table 3 (a–d) present measured quantities as follows:

P_t: critical toppling load (suspended load)

W_t: total weight (suspended load plus crane weight)

h_0: suspended load height before testing

h_1: suspended load height immediately before toppling

Details of the calculation methods are described in Reference 9; a brief summary is provided here. The structural model used in the stability analysis is a simple rigid-bar–rotational-spring system, as illustrated in Figure 4 [10]. The toppling condition is expressed by the following equation [8]:

Table 3-1: Results of Basic Toppling Experiments: A. on PC.

A. On PC		Toppling Ecperiments						Numerical Analyses					
Row No.	Item	[1] θ_{o1}=30deg.			[2] θ_{o2}=45deg.			[1'] θ_{o1}=30deg.			[1"] θ_{o1}=30deg.		
		A1	A2	A3	A4	A5	A6	A1'	A2'	A3'	A1"	A2"	A3"
(a)	P (gf)	5.8	8.7	11.7	3.3	4.7	6.5	3.3	4.7	6.5	3.3	4.7	6.5
(b)	Wt (gf)	71.3	74.2	77.2	68.8	70.2	72	68.8	70.2	72	68.8	70.2	72
(c)	h_0 (cm)	24	18	14.3	19.5	15.3	12	24	18	14.3	24	18	14.3
(d)	h1 (cm)	23.8	17.97	14.29	19.3	14.8	11.7	23.9	17.98	14.295	23.9	17.98	14.295
(e)	L_B (cm)	27.71	20.78	16.51	27.58	21.64	16.97	27.71	20.78	16.51	27.71	20.78	16.51
(f)	a (cm)	13.86	10.39	8.26	19.50	15.30	12.00	13.86	10.39	8.26	13.86	10.39	8.26
(g)	θ_0 (deg.)	30	30	30	45	45	45	30	30	30	30	30	30
(h)	θ_0 (rad.)	0.5236	0.5236	0.5236	0.7854	0.7854	0.7854	0.5236	0.5236	0.5236	0.5236	0.5236	0.5236
(i)	g (cm)	3.300	3.300	3.300	3.300	3.300	3.300	2.856	2.802	2.823	2.856	2.802	2.823
(j)	e (cm)	1.650	1.650	1.650	1.650	1.650	1.650	1.206	1.152	1.173	1.206	1.152	1.173
(k)	L= e/sin θ o (cm)	3.300	3.300	3.300	2.333	2.333	2.333	2.413	2.304	2.346	2.413	2.304	2.346
(l)	θ u (rad.)	0.538	0.526	0.525	0.796	0.818	0.810	0.818	0.772	0.791	0.818	0.772	0.791
(m)	θ_0 / θ u	0.973	0.995	0.998	0.987	0.961	0.970	0.640	0.678	0.662	0.640	0.678	0.662
(n)	Pu/Pcr = $1-\theta_0/\theta$ u	0.027	0.005	0.002	0.013	0.039	0.030	0.360	0.322	0.338	0.026	0.005	0.002
(o)	Pcr (gf)	2690	13566	33485	5364	1784	2362	191	218	213	2690	13566	33485
(p)	Ks (gf*cm)	8876	44768	110500	12517	4163	5511	461	502	500	8876	44768	110500
(q)	S/2 (cm)	1.65	1.65	1.65	1.65	1.65	1.65	1.65	1.65	1.65	1.65	1.65	1.65
(r)	e_M (cm)	0.5691	0.4888	0.4700	0.7507	0.6705	0.6229	0.5691	0.4888	0.4700	0.5691	0.4888	0.4700
(s)	L_M (cm)	1.1382	0.9776	0.9399	1.0616	0.9483	0.8809	1.1382	0.9776	0.9399	1.1382	0.9776	0.9399
(t)	kv (gf/cm)	1630	8222	20294	2299	765	1012	85	92	92	1630	8222	20294
(u)	d (cm)	0.0437	0.0090	0.0038	0.0299	0.0918	0.0711	0.7027	0.6464	0.6706	0.0365	0.0072	0.0030
(v)	Mt (gf*cm)	117.6	122.4	127.4	113.5	115.8	118.8	83.0	80.9	84.4	83.0	80.9	84.4
(w)	R_A (gf)	0.0	0.0	0.0	0.0	0.0	0.0	9.2	10.6	10.4	9.2	10.6	10.4
(x)	R_B (gf)	71.3	74.2	77.2	68.8	70.2	72.0	59.6	59.6	61.6	59.6	59.6	61.6
(y)	Pa (gf*cm)	80.4	90.4	96.6	64.4	71.9	78.0	45.7	48.8	53.7	45.7	48.8	53.7

Table 3-2: Results of Basic Toppling Experiments: A. on Mattress.

B. On Mattress		Toppling Ecperiments						Numerical Analyses					
Row No.	Item	[1] θ_{o1} = 30deg.			[2] θ_{o2} = 45deg.			[1'] θ_{o1} = 30deg.			[1''] θ_{o1} = 30deg.		
		B1	B2	B3	B4	B5	B6	B1'	B2'	B3'	B1''	B2''	B3''
(a)	P (gf)	5.7	7.8	11.7	3.1	4.1	6	3.1	4.1	6	3.1	4.1	6
(b)	Wt (gf)	71.2	73.3	77.2	68.6	69.6	71.5	68.6	69.6	71.5	68.6	69.6	71.5
(c)	h_0 (cm)	23.9	17.9	14.3	18.3	14	11.3	23.9	17.9	14.3	23.9	17.9	14.3
(d)	h1 (cm)	23.5	17.3	14	17.8	13.9	11.2	23.7	17.7	14.2	23.7	17.7	14.2
(e)	L_B (cm)	27.60	20.67	16.51	25.88	19.80	15.98	27.60	20.67	16.51	27.60	20.67	16.51
(f)	a (cm)	13.80	10.33	8.26	18.30	14.00	11.30	13.80	10.33	8.26	13.80	10.33	8.26
(g)	θ_0 (deg.)	30	30	30	45	45	45	30	30	30	30	30	30
(h)	θ_0 (rad.)	0.5236	0.5236	0.5236	0.7854	0.7854	0.7854	0.5236	0.5236	0.5236	0.5236	0.5236	0.5236
(i)	g (cm)	3.300	3.300	3.300	3.300	3.300	3.300	2.835	2.832	2.773	2.835	2.832	2.773
(j)	e (cm)	1.650	1.650	1.650	1.650	1.650	1.650	1.185	1.182	1.123	1.185	1.182	1.123
(k)	L= e/sin θ o (cm)	3.300	3.300	3.300	2.333	2.333	2.333	2.370	2.364	2.247	2.370	2.364	2.247
(l)	θ u (rad.)	0.552	0.579	0.559	0.812	0.793	0.794	0.801	0.798	0.746	0.801	0.798	0.746
(m)	θ_0 / θ u	0.949	0.904	0.937	0.967	0.991	0.989	0.654	0.656	0.702	0.654	0.656	0.702
(n)	Pu/Pcr = 1-θ_0 / θ u	0.051	0.096	0.063	0.033	0.009	0.011	0.346	0.344	0.298	0.049	0.091	0.058
(o)	Pcr (gf)	1389	766	1223	2067	7750	6445	198	202	240	1389	766	1223
(p)	Ks (gf/cm)	4582	2527	4037	4823	18084	15039	470	478	539	4582	2527	4037
(q)	S/2 (cm)	1.65	1.65	1.65	1.65	1.65	1.65	1.65	1.65	1.65	1.65	1.65	1.65
(r)	e_M (cm)	0.5928	0.6158	0.4700	0.8620	0.8769	0.7660	0.5878	0.6089	0.4700	0.5878	0.6089	0.4700
(s)	L_M (cm)	1.1856	1.2316	0.9399	1.2190	1.2402	1.0833	1.1755	1.2179	0.9399	1.1755	1.2179	0.9399
(t)	kv (gf/cm)	842	464	741	886	3321	2762	86	88	99	842	464	741
(u)	d (cm)	0.0846	0.1579	0.1041	0.0774	0.0210	0.0259	0.6828	0.6799	0.6072	0.0700	0.1287	0.0810
(v)	Mt (gf/cm)	117.5	120.9	127.4	113.2	114.8	118.0	81.3	82.3	80.3	81.3	82.3	80.3
(w)	R_A (gf)	0.0	0.0	0.0	0.0	0.0	0.0	9.7	9.9	11.4	9.7	9.9	11.4
(x)	R_B (gf)	71.2	73.3	77.2	68.6	69.6	71.5	58.9	59.7	60.1	58.9	59.7	60.1
(y)	Pa (gf/cm)	78.7	80.6	96.6	56.7	57.4	67.8	42.8	42.4	49.5	42.8	42.4	49.5

Table 3-3: Results of Basic Toppling Experiments: A. on Towel.

C. On Towel		Toppling Ecperiments						Numerical Analyses					
Row No.	Item	[1] θ_{o1} = 30deg.			[2] θ_{o2} = 45deg.			[1'] θ_{o1} = 30deg.			[1''] θ_{o1} = 30deg.		
		C1	C2	C3	C4	C5	C6	C1'	C2'	C3'	C1''	C2''	C3''
(a)	P (gf)	3.4	5.5	7.3	2	3	4	2	3	4	2	3	4
(b)	Wt (gf)	68.9	71	72.8	67.5	68.5	69.5	67.5	68.5	69.5	67.5	68.5	69.5
(c)	h_0 (cm)	23.8	17.7	14.2	17.3	14.3	11.9	23.8	17.7	14.2	23.8	17.7	14.2
(d)	h1 (cm)	22.3	16.9	13.2	16.5	13	10.6	23	17	14	23	17	14
(e)	L_B (cm)	27.48	20.44	16.40	24.47	20.22	16.83	27.48	20.44	16.40	27.48	20.44	16.40
(f)	a (cm)	13.74	10.22	8.20	17.30	14.30	11.90	13.74	10.22	8.20	13.74	10.22	8.20
(g)	θ_0 (deg.)	30	30	30	45	45	45	30	30	30	30	30	30
(h)	θ_0 (rad.)	0.5236	0.5236	0.5236	0.7854	0.7854	0.7854	0.5236	0.5236	0.5236	0.5236	0.5236	0.5236
(i)	g (cm)	3.300	3.300	3.300	3.300	3.300	3.300	3.049	2.987	2.989	3.049	2.987	2.989
(j)	e (cm)	1.650	1.650	1.650	1.650	1.650	1.650	1.399	1.337	1.339	1.399	1.337	1.339
(k)	L= e/sin θ o (cm)	3.300	3.300	3.300	2.333	2.333	2.333	2.798	2.675	2.678	2.798	2.675	2.678
(l)	θ u (rad.)	0.624	0.597	0.635	0.831	0.873	0.889	0.940	0.906	0.907	0.940	0.906	0.907
(m)	θ_0 / θ u	0.839	0.877	0.824	0.946	0.900	0.883	0.557	0.578	0.577	0.557	0.578	0.577
(n)	Pu/Pcr = 1-θ_0 / θ u	0.161	0.123	0.176	0.054	0.100	0.117	0.443	0.422	0.423	0.158	0.119	0.168
(o)	Pcr (gf)	428	576	415	1239	685	594	152	162	164	428	576	415
(p)	Ks (gf/cm)	1411	1900	1369	2892	1599	1387	426	434	440	1411	1900	1369
(q)	S/2 (cm)	1.65	1.65	1.65	1.65	1.65	1.65	1.65	1.65	1.65	1.65	1.65	1.65
(r)	e_M (cm)	1.022	0.930	0.920	1.172	1.071	1.024	1.022	0.930	0.920	1.022	0.930	0.920
(s)	L_M (cm)	2.045	1.861	1.840	1.658	1.514	1.448	2.045	1.861	1.840	2.045	1.861	1.840
(t)	kv (gf/cm)	259	349	251	531	294	255	78	80	81	259	349	251
(u)	d (cm)	0.2659	0.2035	0.2896	0.1271	0.2332	0.2729	0.7966	0.7778	0.7785	0.2407	0.1777	0.2504
(v)	Mt (gf/cm)	113.7	117.2	120.1	111.4	113.0	114.7	94.4	91.6	93.1	94.4	91.6	93.1
(w)	R_A (gf)	0.0	0.0	0.0	0.0	0.0	0.0	5.1	6.5	6.5	5.1	6.5	6.5
(x)	R_B (gf)	68.9	71.0	72.8	67.5	68.5	69.5	62.4	62.0	63.0	62.4	62.0	63.0
(y)	Pa (gf/cm)	46.7	56.2	59.8	34.6	42.9	47.6	27.5	30.7	32.8	27.5	30.7	32.8

Table 3-4: Results of Basic Toppling Experiments: A. on Cushion.

D. On Cushion		Toppling Ecperiments						Numerical Analyses					
Row No.	Item	[1] θ_{o1}=30deg.			[2] θ_{o2}=45deg.			[1'] θ_{o1}=30deg.			[1''] θ_{o1}=30deg.		
		D1	D2	D3	D4	D5	D6	D1'	D2'	D3'	D1''	D2''	D3''
(a)	P (gf)	2.5	4	7	2.5	3.7	4.7	2.5	3.7	4.7	2.5	3.7	4.7
(b)	Wt (gf)	68	69.5	72.5	68	69.2	70.2	68	69.2	70.2	68	69.2	70.2
(c)	h_0 (cm)	23.7	18	14.1	19.8	15.3	12.5	23.7	18	14.1	23.7	18	14.1
(d)	h1 (cm)	22	16	13.5	17.5	13.5	11	23	17	14	23	17	14
(e)	L_B (cm)	27.37	20.78	16.28	28.00	21.64	17.68	27.37	20.78	16.28	27.37	20.78	16.28
(f)	a (cm)	13.68	10.39	8.14	19.80	15.30	12.50	13.68	10.39	8.14	13.68	10.39	8.14
(g)	θ_0 (deg.)	30	30	30	45	45	45	30	30	30	30	30	30
(h)	θ_0 (rad.)	0.5236	0.5236	0.5236	0.7854	0.7854	0.7854	0.5236	0.5236	0.5236	0.5236	0.5236	0.5236
(i)	g (cm)	3.300	3.300	3.300	3.300	3.300	3.300	3.294	3.262	3.076	3.294	3.262	3.076
(j)	e (cm)	1.650	1.650	1.650	1.650	1.650	1.650	1.644	1.612	1.426	1.644	1.612	1.426
(k)	L= e/sin θ o (cm)	3.300	3.300	3.300	2.333	2.333	2.333	3.287	3.224	2.852	3.287	3.224	2.852
(l)	θ u (rad.)	0.637	0.692	0.593	0.896	0.897	0.899	1.045	1.034	0.954	1.045	1.034	0.954
(m)	$\theta_0 / \theta u$	0.822	0.756	0.883	0.877	0.876	0.873	0.501	0.507	0.549	0.501	0.507	0.549
(n)	Pu/Pcr = $1-\theta_0/\theta u$	0.178	0.244	0.117	0.123	0.124	0.127	0.499	0.493	0.451	0.178	0.243	0.114
(o)	Pcr (gf)	382	285	618	552	556	555	136	140	156	382	285	618
(p)	Ks (gf*cm)	1261	941	2040	1288	1297	1295	448	452	444	1261	941	2040
(q)	S/2 (cm)	1.65	1.65	1.65	1.65	1.65	1.65	1.65	1.65	1.65	1.65	1.65	1.65
(r)	e_M (cm)	1.191	1.116	0.956	0.957	0.879	0.871	1.184	1.116	0.944	1.184	1.116	0.944
(s)	L_M (cm)	2.381	2.232	1.913	1.354	1.243	1.232	2.368	2.232	1.888	2.368	2.232	1.888
(t)	kv (gf/cm)	232	173	375	237	238	238	82	83	82	232	173	375
(u)	d (cm)	0.2937	0.4020	0.1935	0.2874	0.2904	0.2953	0.8248	0.8237	0.8027	0.2931	0.3957	0.1747
(v)	Mt (gf*cm)	112.2	114.7	119.6	112.2	114.2	115.8	111.8	111.6	100.1	111.8	111.6	100.1
(w)	R_A (gf)	0.0	0.0	0.0	0.0	0.0	0.0	0.1	0.8	4.8	0.1	0.8	4.8
(x)	R_B (gf)	68.0	69.5	72.5	68.0	69.2	70.2	67.9	68.4	65.4	67.9	68.4	65.4
(y)	Pa (gf*cm)	34.2	41.6	57.0	49.5	56.6	58.8	34.2	38.5	38.3	34.2	38.5	38.3

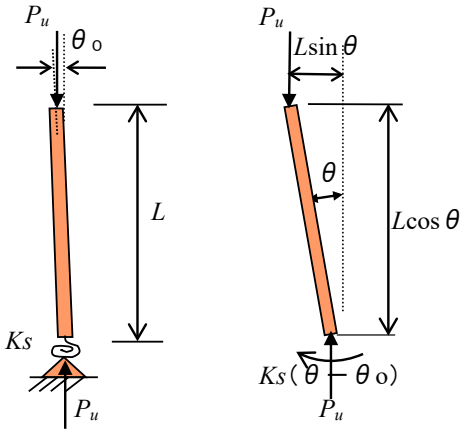

Figure 4: Structural Model for Crane.

$$\frac{P_u}{P_{cr}} + \frac{\theta_0}{\theta_u} = 1$$

where $P_u = W_t$ is the total weight P_{cr} is the elastic limit load (K_s/L), θ_0 is the initial boom inclination angle, θ_u is the overturning angle, K_s is the rotational spring stiffness, and L is the member length from the support point to the center of mass of P_u. In Table 3, g denotes the horizontal distance from the reaction point R_A to the total weight, and e denotes the horizontal distance from the rotation center to the total weight ($e = g - s/2$); see Figure 5 for geometric definitions). Note that P_u in Equation (1) represents the total load used to evaluate the contribution of structural instability, which differs from the suspended load P_t. For simplicity, the support point is assumed at the midpoint between the left and right crawlers, with the boom rotation center coincident with the support point.

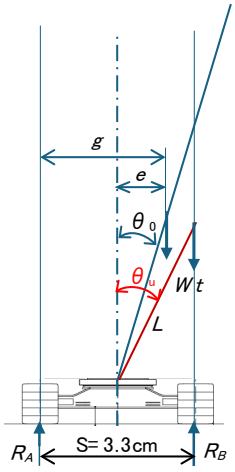

Figure 5: Geometric Configuration.

According to the overturning-moment-dominated criterion, toppling occurs when the overturning moment exceeds the resisting moment [4]. In this case, as shown in Figure 5, the total weight W_t is aligned vertically with the crawler reaction $R_B(R_B = W_t, R_A = 0)$. From the geometry, g=S and e=S/2 at toppling, which allows determination of the member length L and the toppling angle θ_u. In experimental columns [1] and [2] of Tables 3-1 to 3-4, the measured toppling load (row a) was used with Equation (1) to estimate the rotational spring stiffness K_s at toppling (row p; see Reference 9 for details).

The crane weight excluding the suspended load is denoted as W_M, and its center-of-mass position e_M is calculated from experimental measurements using the following equation:

$$e_M = \frac{W_t \cdot S/2 - P_t \cdot a}{W_M} \qquad (2)$$

where e_M is the horizontal distance from the midpoint between the crawlers to the crane center of mass, P_t is the suspended load, and a is the working radius of the suspended load. Other foundation-related parameters in Table 3 include k_v, the foundation reaction coefficient (load per unit settlement), and $d = R_B/k_v$, the foundation settlement.

A comparison of experimental columns [1] (θ_0 = 30°) and [2] (θ_0 = 45°) shows that, as expected, the larger initial inclination in [2] results in a larger working radius and therefore a smaller critical toppling load. In Table 3-1 (A. on laptop computer), the contribution ratio of structural instability (P_u/P_{cr}, row n) is very small compared to the overturning-moment contribution (θ_0/θ_u, row m). This is consistent with the very stiff foundation, where P_{cr} approaches infinity, making the overturning-moment effect dominant.

Figure 6 presents the stability diagrams for each basic toppling experiment, showing the contribution ratios of structural instability and overturning moment based on Equation (1) [8]. The vertical axis represents P_u/P_{cr}, while the horizontal axis represents θ_0/θ_u. The diagonal line indicates the neutral boundary between stable and unstable conditions, namely toppling. Experimental results on relatively stiff foundations ([1] A1–A6, [2] B1–B6) cluster near the horizontal axis $(\theta_0/\theta_u \approx 1)$, indicating overturning-moment-dominated behavior (in green ellipse). Results on relatively soft foundations ([1] C1–C6, [2] D1–D6) plot higher, corresponding to equilibrium-transition-type toppling (in red ellipse). In all cases, the contribution of structural instability remains small due to the characteristics of the supporting foundation.

Discussion of Lower Load Cases

The simulation column [1′] in the right portion of Table 3-1 represents the "toppling condition" calculated for an initial boom inclination angle of θ_0 = 30° (same as column [1]), but with a suspended load smaller than the measured toppling load in [1], set equal to the smaller value in column [2]. Under this condition, toppling requires a weaker supporting foundation due to the reduced load, resulting in a smaller rotational spring stiffness compared to columns [1] and [2].

For example, at load point A1′, the contribution ratio for toppling according to Equation (1) is $\frac{P_u}{P_{cr}} + \frac{\theta_0}{\theta_u} = 0.360 + 0.640 = 1.0$. Compared with the measured case [1] A1 (0.027+0.973=1.0), the contribution of structural instability (first term) is significantly higher due to the weaker foundation. In the stability diagram of Figure 6, this condition lies on the diagonal boundary but shifts toward the center (green long-dashed ellipse). Here, the reaction R_A (row w) is nonzero, and the total weight and reaction are not aligned vertically as in overturning-moment-dominated cases (Figure 5). Therefore, toppling in this case is primarily induced by structural instability due to the compliant foundation. Similar trends are observed for the load points A2′ and A3′.

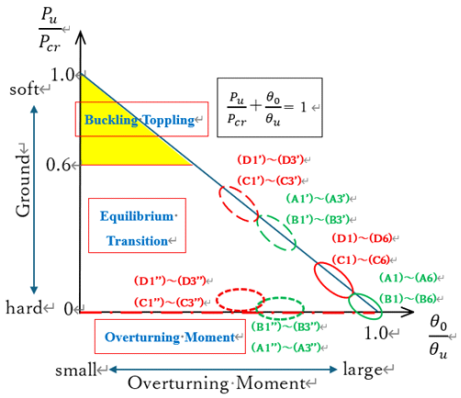

Figure 6: Toppling Stability Diagram.

Next, in the simulation column [1″] at the far right, the foundation stiffness is kept equal to the hard value in [1], while the suspended load is reduced to the smaller value in [2]. That is, the supporting foundation is rigid, but the load is smaller, providing a margin against overturning. At load point A1″, the overturning contribution ratio is $\frac{P_u}{P_{cr}}+\frac{\theta_0}{\theta_u}=0.026+0.640=0.666(<1.0)$ indicating that the toppling condition is not met. Compared with the measured experiment [1] A1 on the laptop computer, the contribution from structural instability (first term) remains almost the same, but the overturning-moment contribution (second term) decreases. On the stability diagram (Figure 6), this condition plots near the horizontal axis (green dotted ellipse), inside the neutral diagonal line, indicating stability and no toppling.

Although this discussion focuses on the A. (on laptop computer foundation), similar trends are observed for other foundation stiffnesses. These results support the rationality of using Equation (1) to evaluate toppling stability from both structural instability and overturning-moment perspectives. It should be noted that the numerical analysis here is based on estimated displacement derived from measured results of experiments [1] and [2], because it is extremely difficult to accurately set and measure both load and displacement in these miniature model experiments. Nevertheless, the estimated values are consistent with experimental behavior, and the qualitative conclusions above are considered valid.

Analysis Based on Toppling Load

The critical overturning load (suspended toppling load) was analyzed using the results of basic experiments [1] and [2] in Tables 3-1 through 3-4. Figure 7 plots the critical loads for the three load points (boom lengths 1, 2, and 3) under all experimental conditions. These load points correspond not only to different boom lengths but also to differences in load height and working radius (Figure 3). In all cases, the shorter the boom, the larger the critical load, because a smaller working radius produces a smaller overturning moment for the same initial boom inclination angle. Figure 7 also shows that the results on relatively stiff foundations (A. on laptop computer and B. on mattress) are similar, whereas the results on softer foundations (C. on towel and D. on cushion) are relatively close to each other. Comparing initial inclination angles θ_0 = 30° (experiment [1], solid lines) and θ_0 = 45° (experiment [2], dashed lines), the difference between the two angles is greater on the stiff foundations (A and B) and smaller on the soft foundations (C and D). This indicates that differences in boom length and supporting foundation stiffness are reflected in the magnitude of the toppling load, likely due to the influence of structural instability.

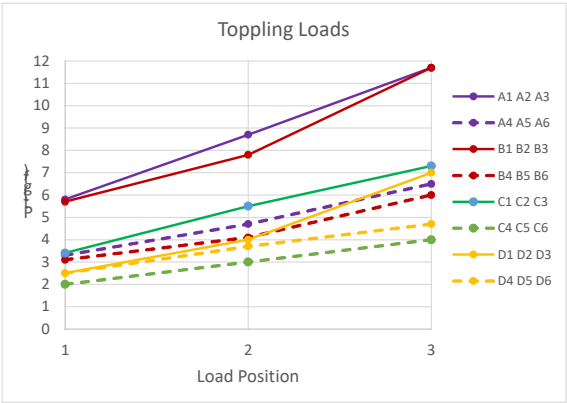

Figure 7: Toppling Load-Boom Length Curves.

Analysis Based on Supporting Foundation Stiffness

Figure 8 plots the rotational spring stiffness K_s against load points 1, 2, and 3 for the basic toppling experiments. The foundation stiffness varies significantly from the stiffest A. on laptop computer to the softest D. on cushion, and this variation is reflected numerically in the K_s values at toppling (row p in Tables 3-1 to 3-4). Specifically, for experiments [1] and [2], K_s is largest on the stiff A. on laptop computer and decreases as the foundation becomes softer. Although the same foundation material should ideally produce consistent values, substantial variability is observed in the experiments, particularly on the relatively stiff A. on laptop computer and B. on mattress, as shown in Figure 8. This variability is attributed to the use of an ultra-small-scale model and analog measurement techniques, which reduce experimental precision.

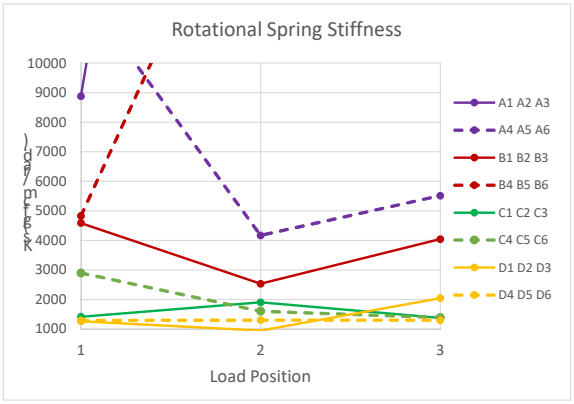

Figure 8: Rotational Stiffness-Boom Length Curves.

The contribution ratios of overturning moment and structural instability, as discussed in Section 4.1 and shown in Figure 6, indicate that the structural instability contribution increases as the foundation becomes softer. In the basic experiments, this contribution remains relatively small—less than 20% even on the softest D. on cushion—with over 80% of toppling attributed to the overturning moment. For the low-load case [1′], achieving toppling requires a very small K_s value (i.e., a highly compliant foundation). Conversely, as illustrated in [1″], if the load is small, toppling is unlikely unless the foundation is extremely soft. This underscores the combined effect of load magnitude and foundation compliance on toppling behavior.

Analysis Based on Overturning Moment

According to the overturning-moment-dominated criterion, toppling occurs when the overturning moment exceeds the resisting moment. The magnitude of the overturning moment at failure is recorded as (row v) in Tables 3-1 through 3-4 for experiments [1] and [2]. Figures 9 and 10 illustrate the relationship between the suspended load and overturning moment for initial boom inclination angles of θ_0 = 30° and 45°, respectively. Each point in the figures represents one of the load points 1, 2, or 3. These points fall along a straight line defined by the following equation:

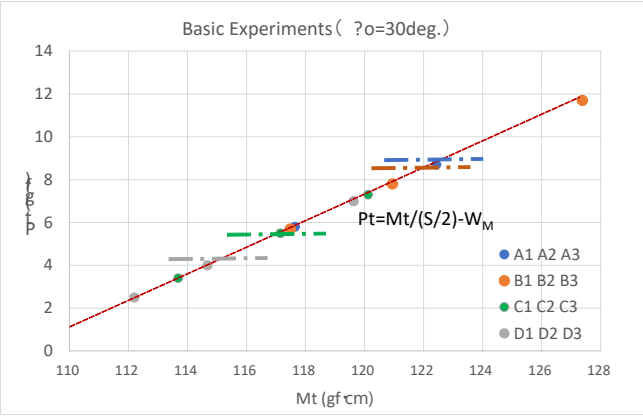

Figure 9: P_t-M_t Curves(θo=3deg).

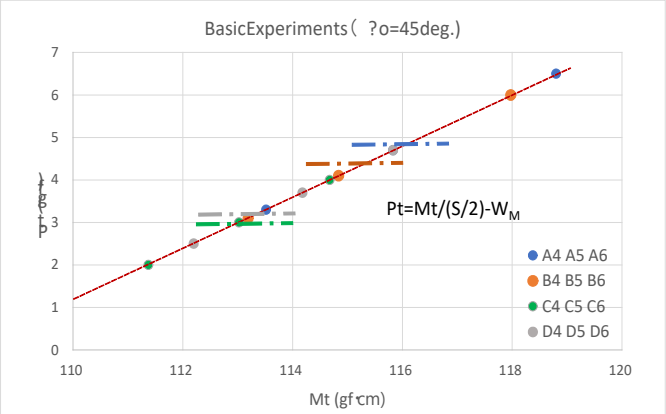

Figure 10: P_t-M_t Curves (θo=45deg).

$$P_t = \frac{M_t}{S/2} - W_M \qquad (3)$$

where P_t is the critical overturning load (suspended toppling load), $M_t = W_t \cdot S/2$ is the overturning moment, S is the crawler spacing, W_t is the total weight (equivalent to P_u), and W_M is the crane body weight. In Figures 9 & 10, the dashed horizontal lines indicate the average values across load points 1, 2, and 3.

From these figures, the effect of foundation type on the overturning moment is negligible for the stiff foundations (A. on laptop computer and B. on mattress), consistent with the minimal differences observed in critical load comparisons. In Figure 10 (θ_0 = 45°), the average M_t for the C. on towel foundation is slightly lower than for the softer D. on cushion, likely due to experimental error, but the difference is minimal.

Examining the effect of initial inclination, in Figure 9 (θ_0 = 30°), tends to increase as the load point moves downward (shorter boom) for all foundation types (A, B, C, D). Because the boom weight is constant in these experiments, this trend is attributed to the influence of structural instability: similar to elastic buckling in slender columns, a shorter boom reduces the contribution of structural instability to toppling, increasing the relative contribution of the overturning moment. In Figure 10 (θ_0 = 45°), a similar trend is observed, but the variation in M_t is smaller. This is consistent with the general observation that structural instability contributes less as the initial inclination increases.

It should be noted that the vertical axes in Figures 9 and 10 represent the suspended load P_t, which differs from the total load P_u used in Equation (1).

Analysis Based on Load Height (Boom Length)

The influence of load height (boom length) was analyzed using the left two columns of the basic toppling experiment results [1] and [2] in Tables 3-1 through 3-4. As shown in Figures 1 & 3, the suspended load height corresponds to load points 1, 2, and 3 (or 4, 5, 6). Naturally, for the same initial boom inclination angle θ_0, shorter boom lengths correspond to smaller working radii and thus larger critical overturning loads (toppling loads). According to the "overturning-moment-dominated" criterion, the overturning moment at failure should theoretically be independent of the load point. However, the experimental results indicate that shorter boom lengths reduce the contribution of structural instability and slightly increase the overturning moment. This trend is more pronounced for smaller initial inclination angles (θ_0 = 30°) than for larger angles (θ_0 = 45°).

Calculation of the Load–Inclination Relationship

To further analyze the relationship between suspended load and overturning, the results of the toppling experiments on the C. on towel foundation (Table 3-3) were used to calculate the boom inclination resulting from a given load. Table 4 extracts the relevant portions of Table 3-3 for this analysis. The inclination θ under suspended load is calculated using the following relationship:

$$\theta = \theta_0 + \frac{P_t \cdot a}{K_s} \qquad (4)$$

where θ_0 is the initial inclination angle, is the working radius, and K_s is the rotational spring stiffness. Note that θ in Equation (4) represents the deformation due to the suspended load P_t only; the crane body weight is not included. The results are plotted in Figure 11, showing, for each experimental case, the initial inclination θ_0 (dotted line), the displacement inclination θ due to the suspended load (solid line), and the overturning inclination θ_u (dashed line). The cases C1–C3 (blue) correspond to θ_0 = 30°, and C4–C6 (brown) correspond to θ_0 = 45°, based on toppling experimental data. Cases C1″–C3″ (green) represent non-toppling simulations with reduced suspended loads.

For C1–C3, the dotted line shows that θ_0 is constant, while the solid line indicates nearly identical deformation inclinations due to the assumption of rigid crane components. The small variation in θ_u (dashed line) is attributed to experimental errors inherent in using the ultra-small-scale model. For C4–C6 (θ_0 = 45°), the

larger initial inclination results in generally larger deformations and rightward shifts in the curves. While the magnitudes of θ, θ_0, and θ_u differ compared to C1–C3, the overall relationships among these angles remain similar. In the case of C1″–C3″ (green), $\theta_0 = 30°$ but the suspended load is small (comparable to the $\theta_0 = 45°$ case), representing non-toppling conditions. Here, the displacement inclination θ is small and nearly identical across load points, while θ_u is larger, indicating significant safety margin against toppling.

Table 4: Loads–Displacement Inclination Angles (Basic Toppling Experiment C: on Towel).

On Towel	30deg.			45deg.			30deg.		
	C1	C2	C3	C4	C5	C6	C1''	C2''	C3''
P (g)	3.4	5.5	7.3	2	3	4	2	3	4
L (cm)	27.48189	20.43821	16.39676	24.46594	20.22329	16.82917	27.48189	20.43821	16.39676
a (cm)	13.74098	10.21913	8.198397	17.30006	14.30005	11.90004	13.74098	10.21913	8.198397
θo	0.5236	0.5236	0.5236	0.7854	0.7854	0.7854	0.5236	0.5236	0.5236
θu	0.624179	0.597255	0.635058	0.830635	0.872618	0.889425	0.940216	0.905954	0.907013
Δθ	0.100579	0.073655	0.111458	0.045235	0.087218	0.104025	0.416616	0.382354	0.383413
Ks (gcm)	1411.027	1899.891	1368.818	2892.255	1599.211	1386.61	1411	1900	1369
θ	0.55671	0.553183	0.567323	0.797363	0.812226	0.819728	0.543077	0.539735	0.547554
Remarks	Toppling (Experimental Results)						Non-Toppling (Numerical)		
	Red: measured, Blue: setup, Green: calculated								

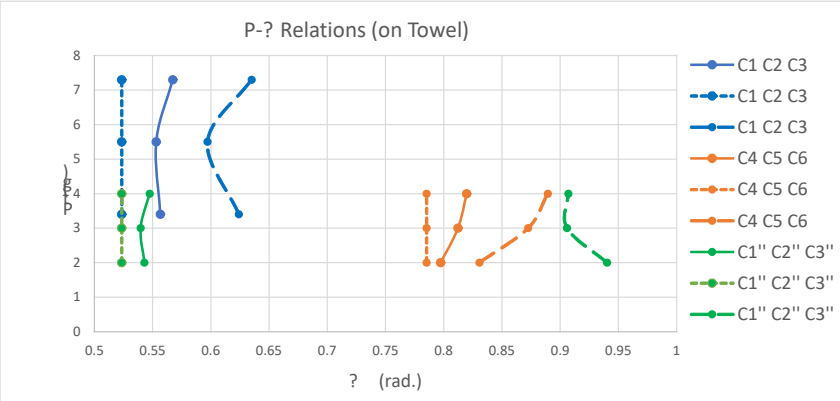

Figure 11: Suspended Loads–Displacement Inclination Angle Curves (Basic Toppling Experiment C).

Results and Discussion of Toppling Experiments for Initial Boom Inclination

To investigate the influence of initial boom inclination on toppling, experiments were conducted on the C. towel foundation with varying initial inclination angles. The results are summarized in Table 5-1, where the blue-shaded cells represent measured values, and the remaining entries represent set or calculated values. The relationship between each initial inclination and the load application point can be seen in Figure 3. The initial inclination $\theta_{02} = 45°$ corresponds to the experimental results from Table 3-3, whereas $\theta_{01} = 30°$, $\theta_{03} = 20°$, and $\theta_{04} = 10°$ were obtained from newly conducted supplementary experiments. Notably, for $\theta_{01} = 30°$, there are slight differences compared to Table 3-1, providing a reference regarding the experimental precision.

Additionally, Table 5-2 presents a comparison of toppling loads including the vertical ($\theta_0 = 0°$) case, and Figure 12 plots these results. For the vertical case, accurate implementation was challenging due to the structural characteristics of the ultra-small-scale model; in practice, the experiment was performed on a slightly inclined surface (see Appendix: Photo 12) as a reference. Although these experiments are limited in precision, they consistently show that toppling load increases as the initial inclination decreases, and also increases as the boom length shortens. As expected, smaller initial inclinations correspond to smaller working radii, resulting in larger toppling loads. Particularly, the difference in toppling load between $\theta_{01} = 30°$ and $\theta_{03} = 20°$ is more pronounced than between $\theta_{03} = 20°$ and $\theta_{04} = 10°$.

Table 5-1: Experimental Results on Effect of Initial Inclination Angles.

Item	[2] θ_{o2} = 45deg.			[1] θ_{o1} = 30deg.			[1] θ_{o3} = 20deg.			[1] θ_{o4} = 10deg.		
	C4	C5	C6	C1	C2	C3	C1	C2	C3	C1	C2	C3
P (gf)	2	3	4	3.1	5.2	7.3	6.7	11.1	17.1	8	12.1	16.2
Wt (gf)	67.5	68.5	69.5	68.6	70.7	72.8	72.2	76.6	82.6	73.5	77.6	81.7
h_0 (cm)	17.3	14.3	11.9	23.8	18.2	14.5	26	20	16	27.2	20.2	15.9
h_1 (cm)	16.5	13	10.6	23.1	17.7	13.8	25.5	19.7	15.6	26.8	20	15.7
L_B (cm)	24.47	20.22	16.83	27.48	21.02	16.74	27.67	21.28	17.03	27.62	20.51	16.15
a (cm)	17.30	14.30	11.90	13.74	10.51	8.37	9.46	7.28	5.82	4.80	3.56	2.80
θ_0 (deg.)	45	45	45	30	30	30	20	20	20	10	10	10
θ_0 (rad.)	0.7854	0.7854	0.7854	0.5236	0.5236	0.5236	0.3491	0.3491	0.3491	0.1745	0.1745	0.1745
g (cm)	3.3	3.3	3.3	3.3	3.3	3.3	3.3	3.3	3.3	3.3	3.3	3.3
e (cm)	1.65	1.65	1.65	1.65	1.65	1.65	1.65	1.65	1.65	1.65	1.65	1.65
L= e/sin θ o (cm)	2.33	2.33	2.33	3.30	3.30	3.30	4.82	4.82	4.82	9.50	9.50	9.50
θ_u (rad.)	0.831	0.873	0.889	0.572	0.569	0.602	0.399	0.388	0.412	0.244	0.224	0.235
θ_0 / θ_u	0.946	0.900	0.883	0.915	0.920	0.870	0.876	0.899	0.847	0.715	0.780	0.741
Pu/Pcr = 1−θ_0 /θu	0.054	0.100	0.117	0.085	0.080	0.130	0.124	0.101	0.153	0.285	0.220	0.259
Pcr (gf)	1239	685	594	803	879	559	582	760	539	258	352	316
Ks(gf∓cm/rad)	2892	1599	1387	2651	2901	1845	2805	3667	2598	2447	3348	3002
S/2 (cm)	1.65	1.65	1.65	1.65	1.65	1.65	1.65	1.65	1.65	1.65	1.65	1.65
e_M (cm)	1.1721	1.0706	1.0240	1.0778	0.9468	0.9009	0.8507	0.6959	0.5603	1.2659	1.2970	1.3648
L_M (cm)	1.6576	1.5141	1.4482	2.1555	1.8936	1.8017	2.4870	2.0344	1.6379	7.2911	7.4703	7.8611
kv (gf/cm)	548	303	263	487	533	339	515	674	477	449	615	551
d (cm)	0.123	0.226	0.265	0.141	0.133	0.215	0.140	0.114	0.173	0.164	0.126	0.148
Mt (gf∓cm)	111.4	113.0	114.7	113.2	116.7	120.1	119.1	126.4	136.3	121.3	128.0	134.8
R_A (gf)	0.0	0.0	0.0	0.0	0.0	0.0	0.0	0.0	0.0	0.0	0.0	0.0
R_B (gf)	67.5	68.5	69.5	68.6	70.7	72.8	72.2	76.6	82.6	73.5	77.6	81.7
Pa (gf∓cm)	34.6	42.9	47.6	42.6	54.6	61.1	63.4	80.8	99.6	38.4	43.1	45.4

Table 5-2: Relations of Suspended Loads to Initial Inclination Angles.

Load position	Experim. case	Initial Inclination, Experim. C: on towel (4 layers)				
		0 deg.	10 deg.	20 deg.	30 deg.	45 deg.
Pt. 1	C1(C4)	30	8	6.7	3.1	2
Pt. 2	C2(C5)	−	12.1	11.1	5.2	3
Pt. 3	C3(C6)	−	16.2	17.1	7.3	4
Remark: Ks=30x27.6=828gfcm/rad. (unit: gf)						

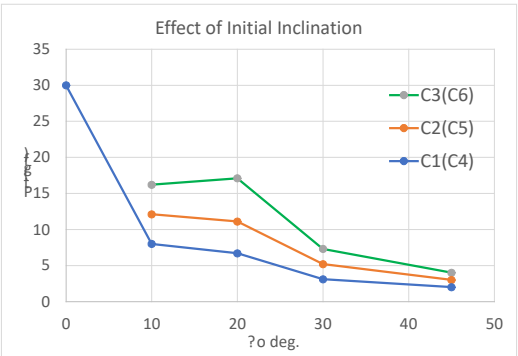

Figure 12: Relations of Suspended Loads to Initial Inclination Angles.

From the overturning characteristics expressed by Equation (1), $\frac{P_u}{P_{cr}}+\frac{\theta_0}{\theta_u}=1$ a clear trend is observed: as the initial inclination decreases, the contribution of structural instability increases. This is due to the relatively soft C. on towel foundation, where loads applied closer to vertical result in higher toppling loads and higher susceptibility to structural instability. A similar trend is observed in the overturning moment M_t. These results confirm the effectiveness and validity of the small-scale toppling experiments for evaluating the influence of initial boom inclination on crane stability.

Results and Discussion of Rotational Spring Stiffness Experiments — Constant Working Radius

Table 6: Ground Stiffness Measurement Results (Fixed Working Radius).

Load pos.	P (gf)	a (cm)	h_0 (cm)	h_1 (cm)	L_B (cm)	a_1 (cm)	θ o deg.	θ_1 deg.	$\Delta\theta$ deg.	Ks (gf·cm/rad.)
C10	4	14.3	22.3	21.2	26.49	15.9	32.7	36.9	4.2	867.7
C2	3.4	14.3	15.3	14.2	20.94	15.4	43.1	47.3	4.3	704.8
C3	3.7	14.3	9	7.9	16.90	14.9	57.8	62.1	4.3	742.8
Setting Values			Measured Values		Caluculated Values				Average	771.8

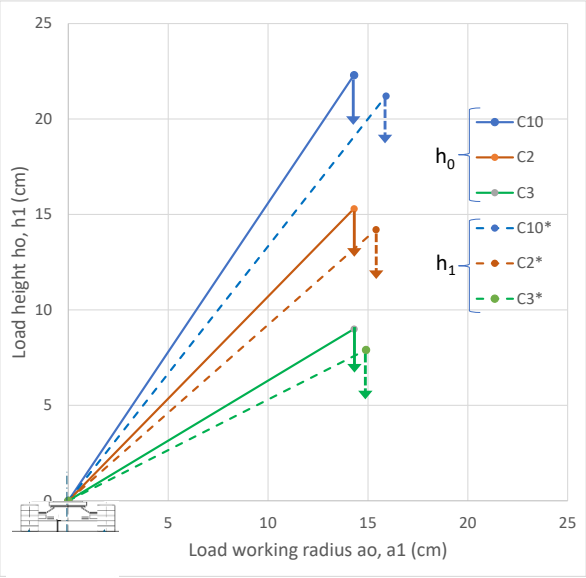

Figure 13: Suspended Loads–Displacement Inclination Angles (Experiment for Ks).

In the basic toppling experiments (Table 3), the calculated rotational spring stiffness K_s exhibited considerable variability. To address this, supplementary experiments were conducted to determine K_s more reliably. These experiments were performed on the C. towel foundation, with the working radius of the suspended load held constant. The load application points were chosen as C10 (an intermediate position between points 1 and 2 at the boom tip for ease of loading), C2, and C3, as illustrated in Figure 13. The experimental conditions and results are summarized in Table 6.

Since the purpose of these experiments was not to induce toppling, the applied loads were selected to be smaller than the corresponding toppling loads. During the experiments, the load heights before and after displacement (h_0 and h_1) were measured to calculate the angular deformation $\Delta\theta$, from which K_s was determined. The calculated values, shown in the rightmost column of Table 6, demonstrate minimal variability among the three load points. The average rotational spring stiffness was determined to be $K_s = 771.8 gf \cdot cm / rad$ which differs significantly from the values obtained in the basic toppling experiments (Table 3-3).

The primary reasons for this discrepancy are as follows. First, in the basic toppling experiments, the initial inclination was set using a protractor, whereas in this supplementary experiment, K_s was calculated based on measured angular displacements. Second, the basic toppling experiments employed the total load P_u and the distance to its center of gravity for calculations, while the current experiment focuses solely on the suspended load. Additional

variability arises from the supporting foundation: the folded towel rested on a hard laptop surface, and variations in towel thickness under prior loading history affected the foundation stiffness. Consequently, the rotational spring stiffness determined in the present experiment is considered more reliable than that obtained in the basic toppling experiments.

Using the K_s values from Table 6, load–displacement curves ($P_t-\theta$ curves) were calculated according to the following expression:

$$P_t = \frac{K_s(\theta-\theta_0)}{L_B \sin\theta} \quad (5)$$

Where L_B is the distance from the rotational center to the suspended load, and the other symbols are defined in Figure 4. Figure 14 presents the resulting $P_t-\theta$ curves for each load point. Because the K_s values are similar, the curves exhibit nearly identical slopes, although the absolute angular displacements differ, as indicated in Figure 13. Furthermore, by applying the average stiffness $K_s = 771.8gf\cdot cm/rad$ to the basic toppling experiments (C1, C2, C3 in Table 3-3), the corresponding $P_t-\theta$ curves were generated, as shown in Figure 15. The intersection of each curve with the respective toppling angle θ_u (dotted lines) provides an estimate of the toppling load. Comparison with the measured toppling loads (dot-dashed lines) demonstrates that, while there are notable differences in magnitude, the overall trends are consistent.

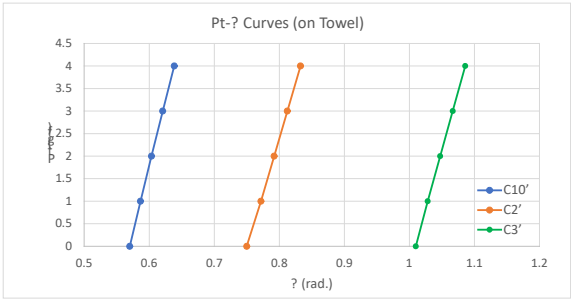

Figure 14: Suspended Loads–Displacement Inclination Angle Curves (C: on Towel).

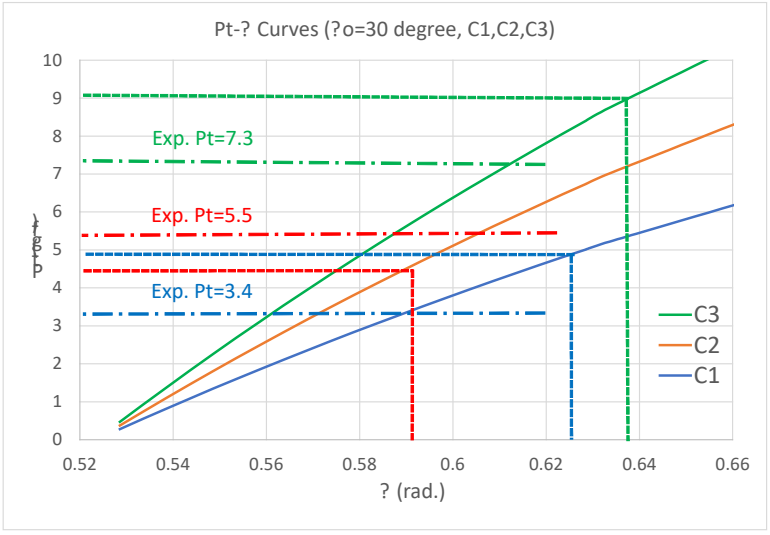

Figure 15: Loads–Displacement Inclination Angle Curves (C: on Towel).

Results and Discussion of Toppling Experiments with Varying Support Foundation Stiffness — Constant Initial Inclination of 10°

The purpose of this experiment was to examine the effects of support foundation stiffness and suspended load height (boom length) on toppling behavior under relatively small initial inclination angles, such as those encountered in pile-driving machines. For this purpose, the initial inclination was held constant at a relatively small 10°, while the support foundation stiffness was varied. Table 7 summarizes the resulting toppling loads (suspended loads) and the corresponding overturning moments.

Table 7: Toppling Experiment Results (Initial Inclination Angle of 10°).

Load Position	Height	Radius	Toppling Load Pt (gf)				Ovrturning Moment Mt (gf*cm)			
	ho (cm)	a (cm)	PC	4枚	6 枚	１０枚	PC	4枚	6 枚	１０枚
1	27.2	4.8	12	7.4	8.1	7.1	57.54	35.5	38.8	34.0
2	20.2	3.6	23	12.5	12.1	10.2	81.903	44.5	43.1	36.3
3	15.9	2.8	32	19.1	17.8	14	89.696	53.5	49.9	39.2

The relationship between initial inclination and load application point is illustrated in Figure 3. Because the initial inclination is constant, the boom length and working radius vary depending on the load application point. Four foundation conditions were considered: a hard laptop surface and 4, 6, or 10 layers of towel on that surface, representing decreasing foundation stiffness. Figures 16 & 17 show the relationships between load height and toppling load, and between load height and overturning moment, respectively. These figures demonstrate a clear difference between the hard laptop surface and the towel foundations. Among the towel conditions, 4- and 6-layer configurations showed minimal difference, whereas the 10-layer configuration exhibited slightly increased foundation softness. The strong similarity between Figures 16 & 17 arises from the linear relationship between toppling load and the corresponding overturning moment namely, moment = load times working radius. Minor discrepancies, such as the 4-layer case producing slightly lower overturning loads and moments than the 6-layer case at load point 1, are attributed to experimental error at small load values. Figure 18 summarizes the toppling load and resulting overturning moment at load points 1, 2, and 3. Because the initial inclination is constant, lower load points correspond to shorter boom lengths and higher toppling loads. The linear relationship between toppling load and moment explains the observed similarity between Figures 16 & 17.

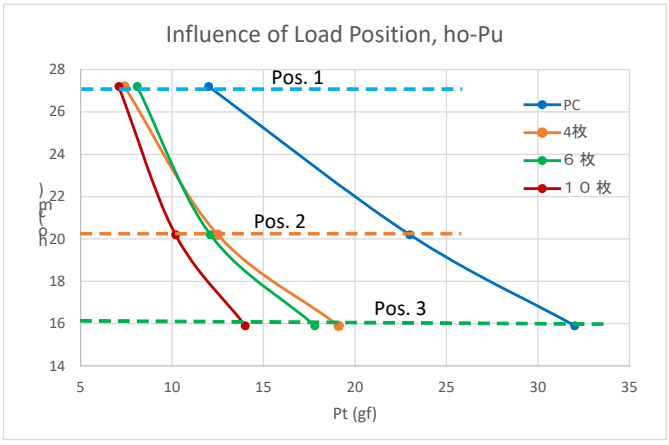

Figure 16: Relationship between Suspended Load Heights and Toppling Loads.

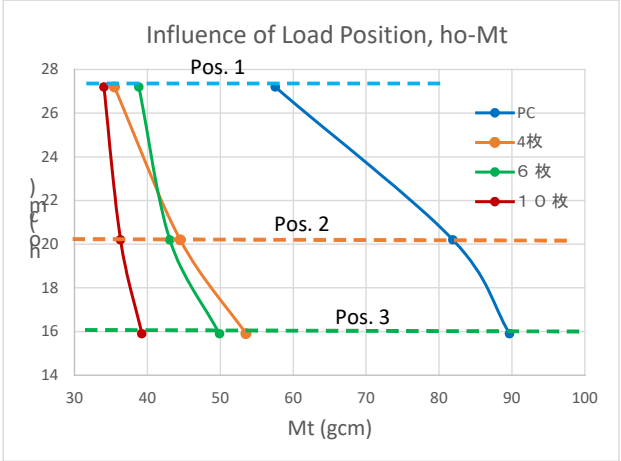

Figure 17: Relationship between Suspended Load Heights and Toppling Moments.

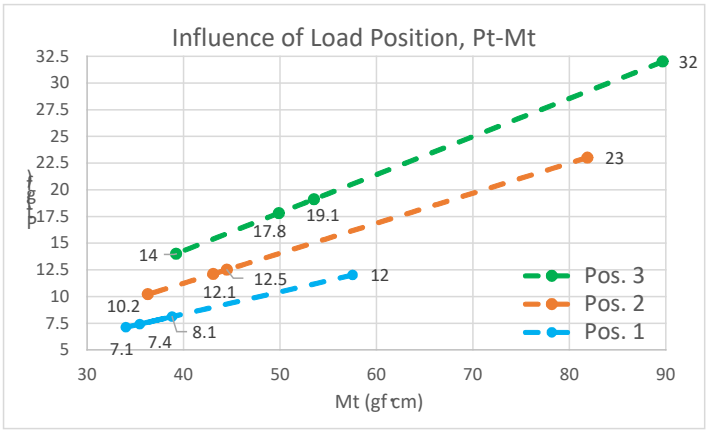

Figure 18: Relationship between Toppling Loads and Toppling Moments.

Results and Discussion of Toppling Experiments with Structural Instability — Balance-Transition Type Toppling

Experimental Results

Structural instability balance-transition type of toppling occurs when structural instability is significant, typically on soft foundations. To investigate this, experiments were conducted on a stiff wooden board and a soft futon to compare toppling behavior. The suspended load was applied at the boom tip (load point 1 in Figure 3), where the effects of structural instability are most pronounced, with a fixed working radius of $a = 8cm$ (corresponding to an initial inclination of 15.7°). The measured toppling loads and other derived results are presented in Table 8 (blue for futon, green for wooden board).

It should be noted that the suspended load P_t differs from the total load $P_u = P_t$ + crane self-weight. The left section of Table 8 lists calculated values assuming the suspended load as the toppling load, following the same geometric relationships described in Figure 5. As expected, larger loads raise the center of gravity, reducing the overturning angle θ_u and increasing the ratio θ_0/θ_u.

The results indicate that the futon (soft foundation) exhibits a lower toppling load (P_t=8.5gf, blue characters) compared with the wooden board (P_t= 11.6gf, red characters). The right section of Table 8 provides the calculated safety margin, defined as $P_u/P_{cr} + \theta_0/\theta_u < 1$, using the rotational spring stiffness K_s or the elastic critical load P_{cr}. This value quantifies the structural reserve against toppling and highlights the increased influence of structural instability on softer foundations.

Table 8: Experimental Results of Equilibrium Toppling.

Pt (gf)	e (cm)	L (cm)	θu (rad.)	θu (deg.)	θo/θu	Pu/Pcr=1−θo/θu	Pcr=Pu/(1−θo/θu)	Ks=Pcr*L	Pu/Pcr	Pu/Pcr+θo/θu	Pu/Pcr	Pu/Pcr+θo/θu
0	0.5290	1.9554	1.0043	57.54	0.2728	0.7272	—		Pcr=6.13E+5(Wood)		Pcr=447.7(Futon)	
1	0.6410	2.3696	0.7702	44.13	0.3557	0.6443	103.2	244.6	0.00011	0.3558	0.1485	0.5042
2	0.7498	2.7715	0.6377	36.54	0.4296	0.5704	118.3	328.0	0.00011	0.4297	0.1508	0.5804
3	0.8553	3.1617	0.5490	31.46	0.4989	0.5011	136.7	432.2	0.00011	0.4991	0.1530	0.6519
4	0.9578	3.5406	0.4848	27.78	0.5651	0.4349	159.8	565.8	0.00011	0.5652	0.1552	0.7203
5	1.0574	3.9088	0.4358	24.97	0.6286	0.3714	189.8	742.0	0.00012	0.6287	0.1575	0.7861
6	1.1543	4.2667	0.3971	22.75	0.6899	0.3101	230.6	983.8	0.00012	0.6900	0.1597	0.8496
7	1.2484	4.6147	0.3656	20.95	0.7492	0.2508	289.1	1334.0	0.00012	0.7493	0.1619	0.9111
8	1.3400	4.9533	0.3396	19.46	0.8066	0.1934	380.1	1882.9	0.00012	0.8068	0.1642	0.9708
8.5	1.3849	5.1191	0.3282	18.80	0.8347	0.1653	447.7	2292.0	0.00012	0.8348	0.1653	1.0000
9	1.4291	5.2827	0.3177	18.20	0.8624	0.1376	541.4	2859.9	0.00012	0.8625	Stability(Futon)	
10	1.5159	5.6035	0.2989	17.13	0.9165	0.0835	904.4	5067.9	0.00012	0.9166		
11	1.6004	5.9158	0.2827	16.20	0.9691	0.0309	2479.1	14665.9	0.00012	0.9693		
11.6	1.6500	6.0993	0.2739	15.70	0.9999	0.0001	612576.8	3.7E+06	0.00013	1.0000		
Toppling Conditions									Stability(Wood)			

Analysis of Overturning Behavior with Varying Support Foundation Stiffness — Contribution of Rotational Spring Stiffness and Load Components

Figure 19 presents the relationship between suspended load P_t (vertical axis) and the contributions of the load term P_u/P_{cr} (purple points) and initial-to-toppling inclination ratio θ_0/θ_u (orange points) on the horizontal axis. The sum of these two contributions reaches unity at toppling, consistent with Eq. (1). From the experiments, the crane model on the futon surface overturns at , corresponding to a calculated rotational spring stiffness of $K_s = 2292gf \cdot cm/rad$. On the stiff wooden board, overturning occurs at P_t= 11.6 gf, yielding $K_s = 3.7\times10^6 gf \cdot cm/rad$. This highlights the large difference in required rotational spring stiffness in order to avoid toppling, despite the relatively modest difference in toppling load.

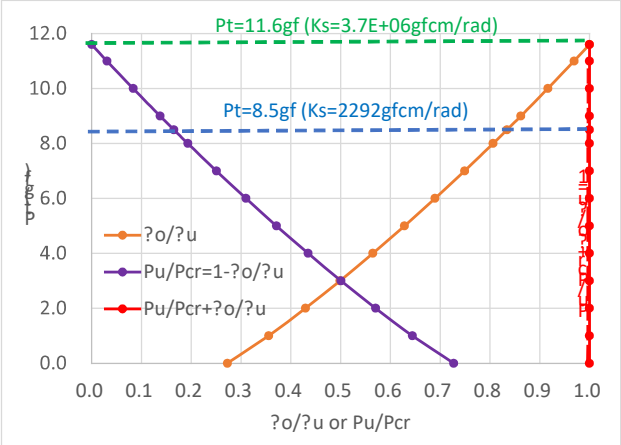

Figure 19: Toppling Contribution Rates.

Figure 20 shows the relationship between P_u/P_{cr} and K_s based on the values from Table 8. Blue solid circles indicate the futon foundation, while green squares represent the wooden board. As the suspended load increases, P_u/P_{cr} decreases because the required increases, thereby increasing the elastic critical load $P_{cr} = K_s/L$. The logarithmic scale of the horizontal axis in Figure 20 emphasizes this effect. Notably, on the wooden board, as the suspended load approaches the toppling load, the required rotational spring stiffness becomes nearly infinite, causing P_{cr} to approach infinity. This illustrates a potential limitation of conventional overturning-moment stability evaluation methods that assume a rigid foundation when encountering unexpectedly soft support conditions. Within the tested range, the reduction in toppling load due to decreased foundation stiffness is relatively modest. Further studies are needed to clarify the relationship between rotational spring stiffness and actual ground stiffness.

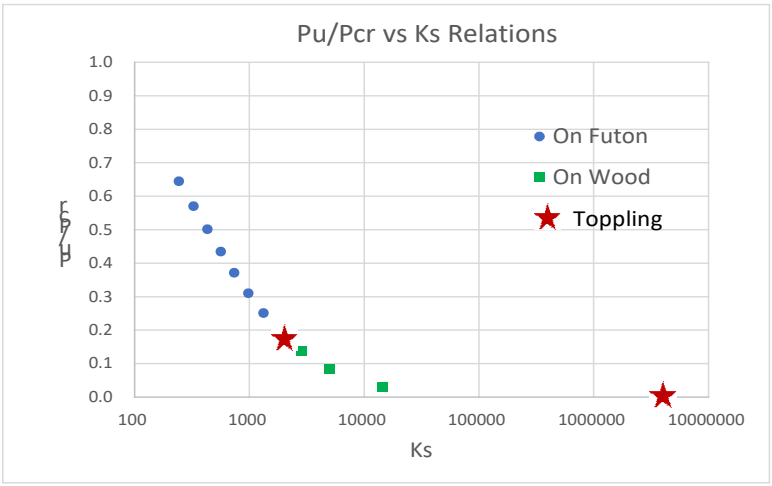

Figure 20: Rotational Stiffness (on Wood & Futon).

Figure 21 plots the contributions of P_u/P_{cr} (vertical axis) and θ_0/θ_u (horizontal axis) against increasing suspended load P_t. Blue circles correspond to the futon surface, and green squares correspond to the wooden board. The intersections of these points with the diagonal line representing the toppling condition Eq. 1, marked by red stars, indicate the values at toppling. It is observed that the contribution of P_u/P_{cr} two toppling is nearly zero on the stiff wooden board, whereas it is approximately 15–17% on the futon.

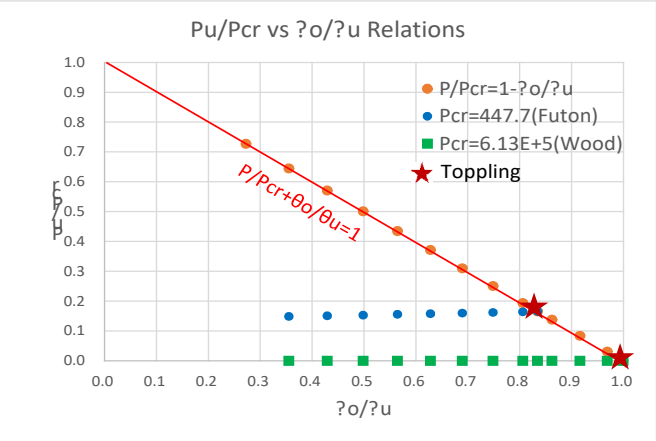

Figure 21: Stability Status (on Wood & Futon).

Figure 22 presents the sum of the contributions $P_u/P_{cr}+\theta_0/\theta_u$ on vertical axis, effectively illustrating the proximity to the toppling condition. Points on the lower part of the figure are the same as those in Figure 21, while the upper points represent their summed contributions. The upper points in Figure 22 allow assessment of the safety margin relative to the toppling condition $P_u/P_{cr}+\theta_0/\theta_u=1.0$. From both Figure 22 and Table 8, it is evident that for the soft futon foundation, the contribution of structural instability to toppling is approximately 16.5%.

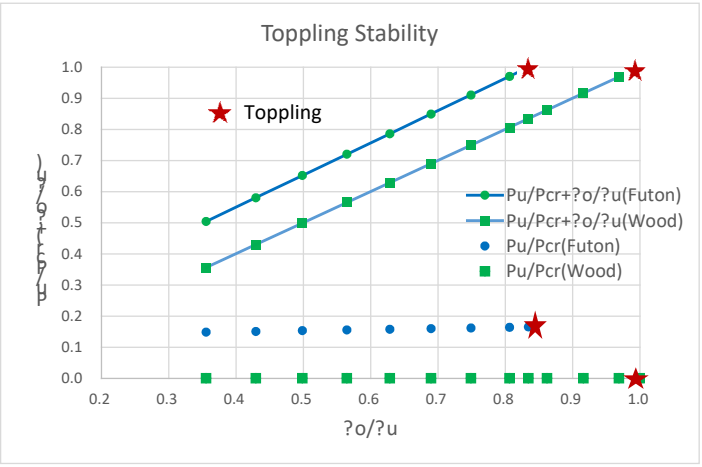

Figure 22: *P/Pcr*+θo/θu (on Wood & Futon).

Conclusions

This study conducted overturning experiments on a miniature crane model to validate the theoretical numerical analyses previously reported by Toma and Chen (2025). The earlier numerical studies investigated toppling conditions by varying factors such as load magnitude and height, foundation stiffness, and initial boom inclination, demonstrating that crane toppling mechanisms are influenced not only by overturning moments but also by structural instability. In the present study, experimental

measurements were conducted under various conditions analogous to the numerical analyses. Comparison of the experimental results with the prior numerical predictions shows good agreement, confirming the involvement of structural instability in the crane toppling behavior. Because the values reported here are based on experimental observations, they provide a practical verification of the overturning stability evaluation methods discussed throughout this research.

However, several limitations must be noted. The experiments employed an ultra-small-scale model, and the analytical structural model—based on rigid bars and rotational springs—represented the entire support system using simplified rotational spring stiffness assumptions. Consequently, the experimental results exhibit relatively large variability. Furthermore, the engineering relationship between the rotational spring stiffness K_s and the actual foundation stiffness remains uncertain. Addressing these issues represents a key direction for future research. To obtain more precise experimental data, larger-scale models combined with high-accuracy digital measurement techniques should be employed. Additionally, collaboration with geotechnical engineers is necessary to clarify the relationship between rotational spring stiffness and actual foundation stiffness, thereby improving the reliability of crane overturning stability assessments.

References

1. Crane Related Accidents-Examples of Disaster, (General Inc. Association) Japan Construction Machinery and Construction Association.
2. Toma S, Chen WF (2022) Overturning Mechanisms of Jacks, Cranes and Pile Driving Machines. Structural Engineering International (SEI), Taylor & Francis Online.
3. Toma S, Chen WF (2022). Some Aspects of Overturning Mechanisms of Pile Driving Machine on Soft Foundation. American Journal of Civil Engineering 10(6): 225-232.
4. Toma S (2024) Model Experiments for Floating Stability of Self-Elevating Platform and Assessment Base on Theory of Structural Stability. Transactions on Engineering and Computer Sciences 2(2).
5. Toma S, Chen WF (2024) Capsizing Mechanism of Self-Elevating Platform Based on Structural Stability Theory. Current Trends Civil & Structural Engineering 11(3).
6. Toma S, Seto K, Chen WF (2023) Dynamic Analysis for Overturning of Pile Driving Machine on Soft Ground. Transactions on Engineering and Computer Sciences 11(2): 61-81.
7. Toma S, Seto K, Chen WF (2024) Comparisons of Static and Dynamic Analyses on Toppling Behaviors of Pile Driving Machinery, etc., on Soft Foundation. Archives of Advanced Engineering Science 2(3): 150-159.
8. Toma S, Chen WF (2024) A Study on Safety Criteria for Toppling of Pile Drivers and Cranes Based on Structural Stability. Archives of Advanced Engineering Science.
9. Toma S, Chen WF (2025) Numerical Study on Toppling Mechanisms of Crane and Pile Driver Based on Structural Stability Theory. Archives of Advanced Engineering Science.
10. Chen WF, Lui, EM (1987) Structural Stability, Theory and Implementation, Chapter 1 General Principles. Elsevier, pp. 12-16.

Appendix

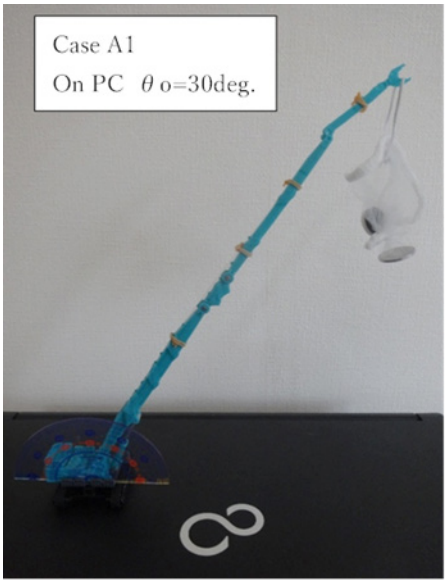

Photo 1: Ultra-small Crane Model (Boom Length 30 cm).

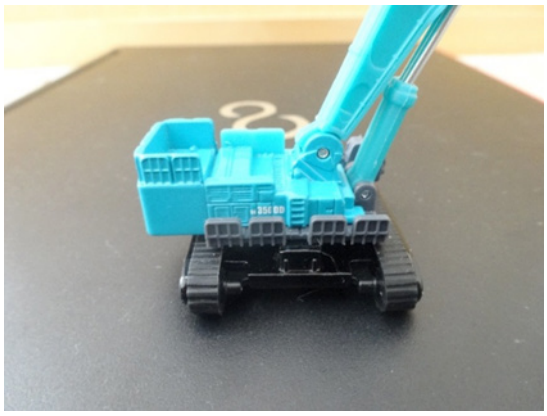

Photo 2: Boom Slewing Direction, 90deg.Crawler spacing 3.3cm).

Photo 3: Mass Scale and Weight.

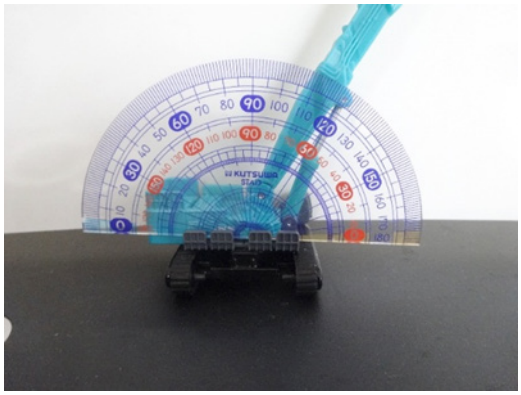

Photo 4: Boom Angle Measurement.

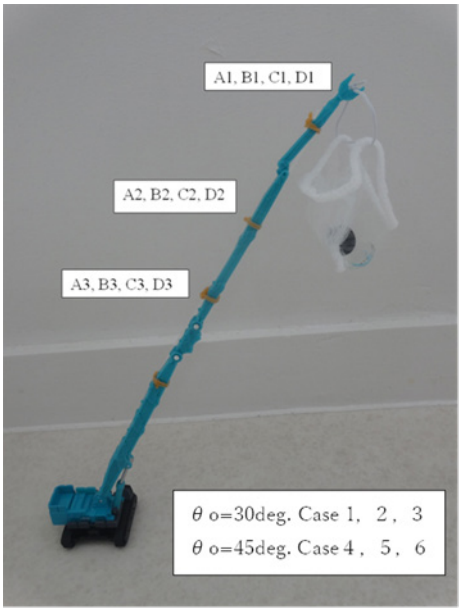

Photo 5: Loading Position and Experiment Cases.

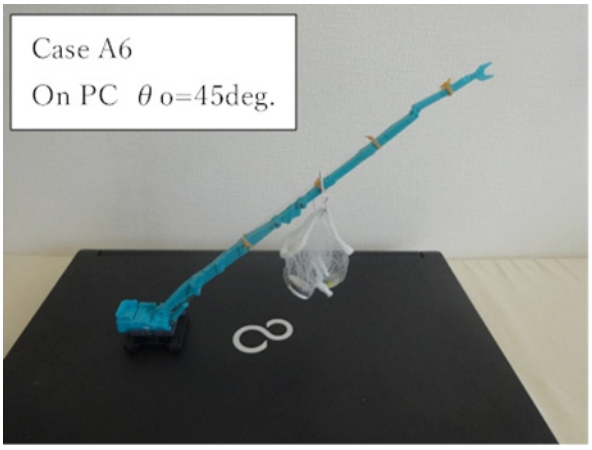

Photo 6: On PC (Case A6).

Photo 7: On Mattress (CaseB2).

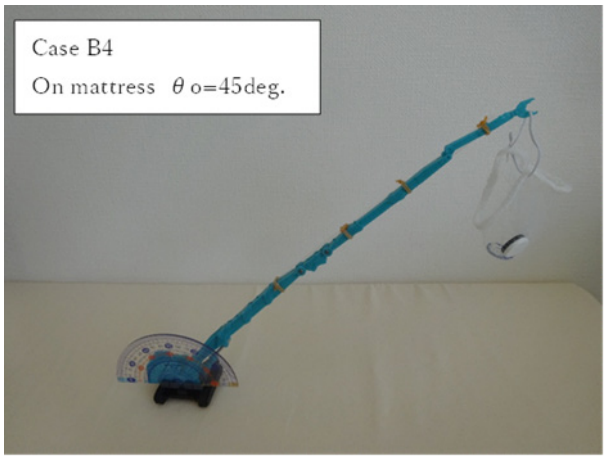

Photo 8: On Mattress (CaseB4).

Photo 9: On Towel (Case C3).

Photo 10: On Cushion (Case D2).

Photo 11: On Towel (Initial Inclination 10deg.).

Photo 12: On Cushion (Upright).